7-7-2008

# Anisoplanatism in Airborne Laser Communication

James A. Louthain [*]
*Air Force Institute of Technology*

Jason D. Schmidt
*Air Force Institute of Technology*



## Recommended Citation

James A. Louthain and Jason D. Schmidt, "Anisoplanatism in airborne laser communication," Opt. Express 16, 10769-10785 (2008).

# Anisoplanatism in airborne laser communication

**James A. Louthain and Jason D. Schmidt**
*Department of Electrical and Computer Engineering*
*Air Force Institute of Technology*
*2950 Hobson Way*
*Wright-Patterson Air Force Base, Ohio 45433-7765*
*james.louthain@afit.edu*

**Abstract:** Airborne laser-communication systems require special considerations in size, complexity, power, and weight. We reduce the variability of the received signal by implementing optimized multiple-transmitter systems to average out the deleterious effects of turbulence. We derive the angular laser-beam separation for various isoplanatic and uncorrelated (anisoplanatic) conditions for the phase and amplitude effects. In most cases and geometries, the angles ordered from largest to smallest are: phase uncorrelated angle (equivalent to the tilt uncorrelated angle), tilt isoplanatic angle, phase isoplanatic angle, scintillation uncorrelated angle, and scintillation correlation angle ($\theta_{\psi_{ind}} > \theta_{TA} > \theta_0 > \theta_{\chi_{ind}} > \theta_{\chi_c}$). Multiple beams with angular separations beyond $\theta_{\chi_c}$ tend to reduce scintillation variations. Larger separations such as $\theta_{TA}$ reduce higher-order phase and scintillation variations and still larger separations beyond $\theta_{\psi_{ind}}$ tend to reduce the higher and lower-order (e.g. tilt) phase and scintillation effects. Simulations show two-transmitter systems reduce bit error rates for ground-to-air, air-to-air, and ground-to-ground scenarios.



**OCIS codes:** (010.1290) Atmospheric optics; (010.1330) Atmospheric turbulence; (060.2605) Free-space optical communication; (060.4510) Optical communications; (070.7345) Wave propagation

## References and links

1. S. M. Haas and J. H. Shapiro, "Capacity of Wireless Optical Communications," IEEE J. Sel. Areas Commun. **21**, 1346–1357 (2003).
2. P. T. Ryan, W. H. Lowrey, I. A. DeLaRue, and R. Q. Fugate, "Scintillation characterization for multiple beams," in *Propagation and Imaging through the Atmosphere III*, M. C. Roggemann and L. R. Bissonnette, eds., vol. 3763, (SPIE Press, Bellingham, WA, 1999) pp. 210–217.
3. P. Polynkin, A. Peleg, L. Klein, T. Rhoadarmer, and J. Moloney, "Optimized multiemitter beams for free-space optical communications through turbulent atmosphere," Opt. Lett **32**, 885–887 (2007).
4. A. Peleg and J. V. Moloney, "Scintillation index for two Gaussian laser beams with different wavelengths in weak atmospheric turbulence," J. Opt. Soc. Am. A **23**, 3114–3122 (2006).
5. I. I. Kim, H. Hakakha, P. Adhikari, E. J. Korevaar, and A. K. Majumdar, "Scintillation reduction using multiple transmitters," Proceedings of SPIE **2990**, 102 (1997).
6. J. A. Anguita, M. A. Neifeld, and B. V. Vasic, "Multi-beam space-time coded systems for optical atmospheric channels," Proceedings of SPIE **6304**, 1–9 (2006).
7. J. A. Anguita, M. A. Neifeld, and B. V. Vasic, "Spatial correlation and irradiance statistics in a multiple-beam terrestial free-space optical communication link" Appl. Opt. **46** 6561–6571 (2007).
8. D. L. Fried, "Anisoplanatism in adaptive optics," J. Opt. Soc. Am. A **72**, 52–61 (1982).
9. R. J. Sasiela, *Electromagnetic wave propagation in turbulence. Evaluation and application of Mellin transforms*, 2nd ed. (SPIE Publications, 2007).

#94855 - $15.00 USD Received 9 Apr 2008; revised 24 Jun 2008; accepted 27 Jun 2008; published 3 Jul 2008

10. R. J. Sasiela and J. D. Shelton, "Transverse spectral filtering and Mellin transform techniques applied to the effect of outer scale on tilt and tilt anisoplanatism," J. Opt. Soc. Am. A **10**, 646660 (1993).
11. J. W. Goodman, *Statistical Optics* (John Wiley & Sons, Hoboken, NJ, 1985).
12. M. C. Roggemann and B. M. Welsh, *Imaging Through Turbulence* (CRC Press, 1996).
13. D. L. Fried, "Optical Resolution Through a Randomly Inhomogeneous Medium for Very Long and Very Short Exposures," J. Opt. Soc. Am. A **56**, 1372–1379 (1966).
14. L. C. Andrews and R. L. Phillips, *Laser Beam Propagation Through Random Media*, 2nd ed. (SPIE Optical Engineering Press Bellingham, WA, 2005).
15. A. D. Wheelon, *Electromagnetic scintillation. 1, Geometrical optics* (Cambridge Univ. Press, 2001).
16. F. D. Eaton and G. D. Nastrom, "Preliminary estimates of the vertical profiles of inner and outer scales from White Sands Missile Range, NM VHF radar observations," Radio Sci. **33**, 859–903 (1998).
17. J. A. Louthain and J. D. Schmidt, "Anisoplanatic Approach to Airborne Laser Communication," (MSS Active E-O Systems Proceedings, Military Sensing Information Analysis Center (SENSIAC), 2007).
18. E. P. Magee, M. R. Whiteley, S. T. Das, and B. M. Welsh, "Tilt anisoplanatism in extended turbulence propagation," Proceedings of SPIE **4976**, 13–21 (2003).
19. D. L. Fried, "Spectral and Angular Covariance of Scintillation for Propagation in a Randomly Inhomogeneous Medium," Appl. Optics **10**, 721–731 (1971).
20. M. C. Roggemann, B. M. Welsh, D. A. Montera, and T. Rhoadarmer, "Method for simulating atmospheric turbulence phase effects for multiple time slices and anisoplanatic conditions," Appl. Opt **34**, 4037–4051 (1995).
21. B. M. Welsh, "Fourier-series-based atmospheric phase screen generator for simulating anisoplanatic geometries and temporal evolution," Proceedings of SPIE **3125**, 327 (1997).
22. J. A. Louthain, "Master's Thesis: Atmospheric turbulence scintillation effects of wavefront tilt estimation," (1997).
23. J. A. Louthain and B. M. Welsh, "Fourier-series-based phase and amplitude optical field screen generator for weak atmospheric turbulence," Proceedings of SPIE **3381**, 286–296 (1998).
24. S. Coy, "Choosing Mesh Spacings and Mesh Dimensions for Wave Optics Simulation," in *Advanced Wavefront Control: Methods, Devices, and Applications III*, J. D. G. Mark T. Gruneisen and M. K. Giles, eds., vol. 5894 (SPIE Press, Bellingham,WA, 2005).
25. Y. Dikmelik and F. M. Davidson, "Fiber-coupling efficiency for free-space optical communication through atmospheric turbulence," Appl. Opt. **44**, 4946–4952 (2005). URL http://ao.osa.org/abstract.cfm?URI=ao-44-23-4946.
26. S. B. Alexander, *Optical Communication Receiver Design*, SPIE Tutorial Texts in Optical Engineering, vol. TT22; IEE Telecommunications Series, vol. 37 (SPIE Press, Bellingham, WA, 1997).
27. L. C. Andrews, R. L. Phillips, and C. Y. Hopen, *Laser Beam Scintillation with Applications*, 2nd ed. (SPIE Press, 2001).
28. E. Dereniak and G. Boreman, *Infrared Detectors and Systems* (Wiley New York, 1996).

## 1. Introduction

Lasers offer tremendous advantages over RF in communication bandwidth and security, due to the ultra-high frequencies and narrow spatial beamwidth of laser propagation. In addition, optical transmitters and receivers are much smaller and lighter than RF versions and operate at much lower power levels. Current airborne sensors are collecting data at an ever-increasing rate. With the advent of hyper-spectral imaging systems, this trend will continue as two-dimensional data is replaced by three-dimensional data cubes at fine resolutions. Current RF communication systems cannot keep up with this trend.

Unfortunately, laser propagation through the air is severely affected by clouds, dust, and atmospheric turbulence, causing long, deep fades at the receiver. The same atmospheric turbulence effects that limit the resolution of optical systems and make the stars twinkle can severely reduce the amount of laser power received. The atmospheric turbulence in the propagation path causes the laser beam to wander, spread, and break up. These effects can cause the received signal power to drop below the receiver's threshold for milliseconds at a time. For a 10 Gbit/s binary laser communication system (LCS), a millisecond fade means millions of bit errors. Since these optical power fades are often very deep, simply turning up the power in this case would not be effective.

There are essentially two different ways to improve this condition: increase the diversity of the signal to average out the effects or compensate for the conditions of the turbulence in real time. In the first case, the temporal and spatial statistics of the turbulence for the propagation

#94855 - $15.00 USD Received 9 Apr 2008; revised 24 Jun 2008; accepted 27 Jun 2008; published 3 Jul 2008

are estimated and techniques are devised to overcome these effects by applying multiple uncorrelated realizations. In the second case, typically, wavefront sensors measure the real-time aberrations of the propagation path, and a closed-loop adaptive optics (AO) system applies a correction to pre-compensate the transmitted beam in real time.

Multiple-transmitter systems increase the diversity of the signal and average out the deleterious effects of turbulence without bulky, complicated AO systems, making it an appropriate choice for airborne laser communications. Through analysis and simulation, we determine optimal configurations for a multiple-transmitter airborne LCS for various geometries and tracking systems.

This research derives the requisite angular and parallel separations for multiple-transmitter systems for airborne and ground-to-ground laser communication. A majority of the previous research on multiple transmitters has focused on satellite communications (in which the turbulence is only present over a short part of the propagation path) or constant-turbulence-strength paths. [1–7] Here, we present these angular separations for three airborne geometries (air-to-air, air-to-ground, and ground-to-air) through extended turbulence and determine practical configurations.

Previous research on isoplanatism has defined the *maximum angle* over which the variance of turbulence effects between two paths is relatively *similar*. [8–10] These isoplanatic angles have been determined for the tilt variance, higher-order phase variance, and scintillation (intensity variance). This research is extended to determine the *minimum angle* at which the paths are relatively *different*. The less correlated the amplitude and phase perturbations are between the paths, the better the averaging effect for multiple beams.

Then, we run simulations to explore how separation distances affect the bit error rate (BER) for multiple-transmitter LCSs. We perform the simulation for multiple scenarios and tracking systems to determine how effective these multiple-transmitter techniques might be for airborne platforms.

## 2. Uncorrelated paths

In this section, we determine the separation required to attain uncorrelated turbulence effects between two laser beam paths. To investigate this, it is instructive to determine when the paths are relatively similar first. If a system effect is space-invariant, it is called isoplanatic. [11] Therefore, if two laser beam paths are considered isoplanatic in terms of any particular turbulence effect, the effects of the two paths are highly correlated.

Most AO systems have a beacon path to measure the turbulence. Sensors at the imaging system or laser transmitter measure how the turbulence affects the beacon. If the differences between the phase effects (wavefront variations) of the propagation path and beacon path are negligible, the phase correction can potentially be implemented effectively. That is to say the phase effects of the paths are isoplanatic. The phase isoplanatic angle $\theta_0$ is the largest angle between two paths for which the wavefront variations in the two paths are relatively similar. [12] If the effects of the paths are significantly different then the paths are anisoplanatic.

There are three different types of isoplanatism of interest in this research: the tilt $\theta_{TA}$, phase $\theta_0$, and scintillation isoplanatic $\theta_{\chi_c}$ angles. Tilt refers to the direction of propagation and deals with tracking a wandering beam or a jittering image. Phase incorporates both the tilt and the higher-order phase aberrations. Scintillation corresponds to the variations in intensity over the pupil. Typically, the tilt isoplanatic angle is larger than the phase isoplanatic angle, which is larger than the scintillation isoplanatic angle. Using these isoplanatic conditions as a starting point, the anisoplanatic conditions are determined for the phase and amplitude effects. The isoplanatic angle $\theta_{TA}$ for a constant turbulence strength profile and the phase independence angle $\theta_{\psi_{ind}}$ are derived for the first time in this section.

#94855 - $15.00 USD Received 9 Apr 2008; revised 24 Jun 2008; accepted 27 Jun 2008; published 3 Jul 2008

The refractive index fluctuations drive the phase and amplitude turbulence effects. For the derivations in this section, we model these fluctuations with the von Kármán power spectral density (PSD) of the refractive index fluctuations [12, 14]

$$\Phi_n(\kappa, z) = \frac{0.033 C_n^2(z)}{(\kappa^2 + \kappa_0^2)^{11/6}}, \tag{1}$$

where $\kappa$ is the 3-D radial spatial frequency and $\kappa_0 = 2\pi/L_0$. This PSD is the most appropriate since it includes the outer scale $L_0$ which limits the size of the large-scale phase effects (i.e. turbulent eddies) which drive the phase anisoplanatic conditions. The refractive index PSD used to derive the isoplanatic conditions consisted of only the numerator in Eq. (1), since the outer-scale does not affect the isoplanatic conditions.

### *2.1. Phase isoplanatism*

Fried derived the phase perturbation structure function in 1966 as [12, 13]

$$\begin{aligned} D_\psi(\Delta\mathbf{x}) &= \mathrm{E}\{[\psi(\mathbf{x}) - \psi(\mathbf{x}+\Delta\mathbf{x})]^2\} && (2)\\ &= 2\Gamma_\psi(0) - 2\Gamma_\psi(\Delta\mathbf{x}), \qquad \text{for stationary random processes,} && (3)\\ &= 2.91 k^2 (\Delta x)^{5/3} \int_0^L C_n^2(z)\, \mathrm{d}z. && (4) \end{aligned}$$

where E is the expectation operator and $\Gamma$ is the auto-correlation. The $\psi$ term denotes the pupil phase perturbation and $C_n(z)^2$ is the strength of turbulence along the path. It can be shown from Eq. (4) that the phase structure function at the receiver for two point sources separated by angle $\theta$ as viewed by the receiver is

$$D_\psi(\theta, L) = 2.91 k^2 [\sin(\theta)]^{5/3} \int_0^L (L-z)^{5/3} C_n^2(z)\, \mathrm{d}z. \tag{5}$$

For this geometry, most of the literature has defined the isoplanatic angle to be the angle at which the structure function is less than or equal to unity. [8, 12, 14] Applying this condition

$$D_\psi(\theta_0, L) = 1 \text{ rad}^2 \tag{6}$$

and solving for the angle results in the familiar isoplanatic angle relation defined by [8]

$$\theta_0 = \left[ 2.91 k^2 \int_0^L C_n^2(z) (L-z)^{5/3} \mathrm{d}z \right]^{-3/5}, \tag{7}$$

where $C_n^2(z)$ is the structure parameter of the turbulence at location $z$ along the path, $L$ is the propagation path length, and $k = 2\pi/\lambda$ is the optical wave number. It is important to note which isoplanatic-angle definition is used. This definition assumes the two point sources are in the $z = 0$ plane. Many definitions in the literature define the $z = 0$ point as the location of the receiver. [9, 12, 14] To adjust, let $z' = L - z$ in Eq. (7).

### *2.2. Angular phase independence of two beams*

Now, we apply these concepts to statistical independence to determine the phase independence angle. The phase structure function in Eq. (5) increases with separation angle, approaching a maximum value at two times the mean square phase or $2\sigma_\psi^2$ as the two paths are placed far apart. This time, we apply the condition for the maximum value for the phase structure function to define $\theta_{\psi_{ind}}$ as the phase independence angle

$$D_\psi(\theta_{\psi_{ind}}, L) = 2\sigma_{\psi,pl}^2. \tag{8}$$

#94855 - $15.00 USD Received 9 Apr 2008; revised 24 Jun 2008; accepted 27 Jun 2008; published 3 Jul 2008

Combining Eqs. (6) and (8) allows us to solve for $\theta_{\psi_{ind}}$, yielding

$$\theta_{\psi_{ind}} = 2\sigma^2_{\psi,pl}\theta_0. \tag{9}$$

Using a geometrical optics plane-wave propagation approximation, the phase variance for a point receiver can be written as [14]

$$\sigma^2_{\psi,pl} \cong 4\pi^2 k^2 \int_0^L \int_0^\infty \kappa \Phi_n(\kappa, z) \mathrm{d}\kappa \, \mathrm{d}z \tag{10}$$

$$= 0.78 k^2 \kappa_0^{-5/3} \int_0^L C_n^2(z) \, \mathrm{d}z. \tag{11}$$

For horizontal propagation (i.e. constant $C_n^2$) the independence angle simplifies to

$$\theta_{\psi_{ind}} = 0.7402 k^{4/5} C_n^{4/5} L^{-3/5} \kappa_0^{-5/3}. \tag{12}$$

This relation for $\theta_{\psi_{ind}}$, first derived here, defines the angle over which the phase effects between the propagation paths of two point sources are nearly uncorrelated. It follows that the phase-independence separation distance can be defined as $d_{\psi_{ind}} = L\theta_{\psi_{ind}}$. As expected, this independence angle increases with outer scale. At this angular separation, the beams should wander independently, and the higher-order phase perturbations should be uncorrelated as well. At this separation a fixed multiple transmitter LCS (e.g. last-mile-type communications) could be designed so that at least one beam with sufficient power remains on the receiver at all times without the need for tracking. This independence angle is highly dependent on the outer scale, which varies near the ground as $L_0 \approx 0.4h$. [15] For example, two $\lambda = 1.55\mu$m transmitters would need to be separated by $d_{\psi_{ind}} = 43$ cm ($\theta_{\psi_{ind}} = 213$ $\mu$rad) for a 2 km path located 1 m above the ground with a turbulence strength of $C_n^2 = 1.71 \times 10^{-14}$ m$^{-2/3}$. For a 4 km path, that separation would need to approach 65 cm.

At high altitudes the effective outer scale is determined by the vertical outer scale and the horizontal outer scale. The vertical outer scale typically varies from 10 to 70 m, [16] while the horizontal outer scale can be much larger. Aircraft measurements have determined the horizontal outer scale can be over hundreds of kilometers. [15] For horizontal propagation simulations in our work at altitude, an infinite outer scale is used because $L_0 \gg D$. When a finite $L_0$ is needed with slant ranges, the effective outer scale is determined by taking a slice through the vertical outer scale

$$L_0 = \frac{L_{0_{vert}}}{\cos \xi}, \tag{13}$$

where $L_{0_{vert}}$ is the outer scale for vertical propagations and $\xi$ is the zenith angle. Both, the outer scale and inner scale $l_0$ vary with altitude. In this research, these bounds on the turbulence are consistent with atmospheric data presented by Wheelon. [15]

### *2.3. Parallel path isoplanatism*

Using Eq. (4) again, we determine the parallel path isoplanatic distance. Now, we look at the phase structure function at the receiver for two point sources separated by $\Delta x$. The structure function for parallel path beams is

$$D_\psi(\Delta x, L) = 2.91 k^2 (\Delta x)^{5/3} \int_0^L C_n^2(z) \, \mathrm{d}z. \tag{14}$$

As we did for the isoplanatic angle condition, we determine the separation $\Delta\mathbf{x_0}$ at which the structure function is unity. The parallel isoplanatic distance is

$$\Delta x_0 = \left[ 2.91 k^2 \int_0^L C_n^2(z) \, \mathrm{d}z \right]^{-3/5} = 0.6611 \rho_0 = 0.3148 r_0, \tag{15}$$

#94855 - $15.00 USD Received 9 Apr 2008; revised 24 Jun 2008; accepted 27 Jun 2008; published 3 Jul 2008

where $\rho_0$ is the spatial coherence radius and $r_0$ is the coherence diameter. [12,14] For a constant $C_n^2(z)$ path

$$\Delta x_0 = 0.5268k^{-6/5}C_n^{-6/5}L^{-3/5} = 0.555L\theta_0. \tag{16}$$

Interestingly enough, this separation is simply $(3/8)^{3/5}$ times the separation for angularly separated paths. Similar to Eq. (8), the plane-wave independent phase separation distance is determined by setting the structure function equal to the maximum value and solving for the separation

$$\Delta x_{ind} = 2\sigma_{\psi,pl}^2\Delta x_0 = 0.4109\kappa_0^{-5/3}\left[k^2\int_0^L C_n^2(z)\,\mathrm{d}z\right]^{2/5}. \tag{17}$$

For a constant $C_n^2$ profile, it simplifies to

$$\Delta x_{ind} = 0.4109k^{4/5}C_n^{4/5}L^{2/5}\kappa_0^{-5/3} = 0.555L\theta_{\psi_{ind}}. \tag{18}$$

### *2.4. Tilt isoplanatism*

Sasiela developed relationships for the differential tilt variance which can also be referred to as the structure function $\sigma_T^2(x) = \mathrm{E}[T(x_1) - T(x_1+x)]^2$ of the Zernike tilt $T$. We use the notation used by Sasiela to allow the reader to follow this work and refer back to Sasiela's. [9] From those relations, he determined a relation for the tilt isoplanatic angle for an astronomical seeing geometry. The refractive index PSD used here does not include the outer scale. Sasiela investigated the effect of outer scale on the tilt isoplanatic angle. The outer scale greatly affects tilt variance, but does not appreciably affect tilt isoplanatism (especially when the outer scale is much larger than the receiver aperture). [10] The differential tilt (i.e. the difference between the Z-tilts) consisted of two contributions: one for $\Delta x < D$ (beams overlap) called the lower contribution and the other for $\Delta x > D$ (beams do not overlap) called the upper contribution, where $D$ is the receiver diameter. The differential tilt variance differs with each axis: the beam displacement axis is denoted by the parallel symbol, and the perpendicular symbol denotes the other axis. This difference in tilt variance can be quite significant [9, 17, 18], but oftentimes these two orientations are added to determine the total differential tilt. The total differential tilt is the sum of the upper and lower contributions for each axis [9]

$$\begin{bmatrix}\sigma_\parallel^2\\ \sigma_\perp^2\end{bmatrix} = \begin{bmatrix}\sigma_\parallel^2\\ \sigma_\perp^2\end{bmatrix}_L + \begin{bmatrix}\sigma_\parallel^2\\ \sigma_\perp^2\end{bmatrix}_U. \tag{19}$$

Now, we derive a closed-form approximation for the differential tilt for a constant $C_n^2$ profile or horizontal propagation, taking into account both the lower ($\Delta x < D$) and upper ($\Delta x > D$) contributions. Starting with $\Delta x < D$, one must only consider the lower contribution for $\theta < D/L$, where $\theta = \Delta x/z$. After performing the integration over $z$ from 0 to the propagation length $L$, the differential tilt becomes

$$\begin{aligned}\begin{bmatrix}\sigma_\parallel^2\\ \sigma_\perp^2\end{bmatrix} = \begin{bmatrix}\sigma_\parallel^2\\ \sigma_\perp^2\end{bmatrix}_L = \frac{6.08C_n^2}{D^{1/3}}\times\Bigg\{&\begin{bmatrix}1.316\\ 0.439\end{bmatrix}\left[\left(\frac{\theta}{D}\right)^2\left(\frac{L^3}{3}\right) - \begin{bmatrix}2.2955\\ 1.377\end{bmatrix}\left(\frac{\theta}{D}\right)^4\left(\frac{L^5}{5}\right)+\cdots\right]\\ &+\begin{bmatrix}2.195\\ 0.388\end{bmatrix}\left[\left(\frac{\theta}{D}\right)^{14/3}\left(\frac{3}{17}\right)L^{17/3} - \begin{bmatrix}0.1756\\ 0.1298\end{bmatrix}\left(\frac{\theta}{D}\right)^{20/3}\left(\frac{3}{23}\right)L^{23/3}+\cdots\right]\Bigg\},\end{aligned} \tag{20}$$

where $\theta_{TA} < D/L$. As $\theta$ approaches zero, the differential variance approaches zero, as expected. To define the tilt isoplanatic angle as Sasiela did, the first term of the infinite sum is set

#94855 - $15.00 USD Received 9 Apr 2008; revised 24 Jun 2008; accepted 27 Jun 2008; published 3 Jul 2008

equal to one half of the diffraction-width angle,

$$\sigma_T^2 = \sigma_\parallel^2 + \sigma_\perp^2 \approx \frac{6.08C_n^2}{D^{1/3}} \times \left[1.755\left(\frac{\theta_{TA}}{D}\right)^2\left(\frac{L^3}{3}\right)\right] = \left(\frac{0.61\lambda}{D}\right)^2. \tag{21}$$

Solving for $\theta_{TA}$, we derived the tilt isoplanatic angle for horizontal propagation as approximately [17]

$$\theta_{TA} = \frac{0.323\lambda D^{1/6}}{C_n L^{3/2}}, \quad \theta < D/L. \tag{22}$$

This straight forward equation for constant turbulence strength can be used to determine the maximum angular separation between the beacon path and the propagation path for $\theta < D/L$ with a tracking system which is important for all our scenarios except the ground-to-ground scenario.

Now, for $\theta > D/L$, following Eq. (19) we must add the significant terms for the lower *and upper* portions to determine the overall differential tilt variance

$$\begin{bmatrix}\sigma_\parallel^2 \\ \sigma_\perp^2\end{bmatrix} \approx \frac{6.08C_n^2}{D^{1/3}}\left\{L\begin{bmatrix}1\\1\end{bmatrix} - \begin{bmatrix}0.7801\\0.9057\end{bmatrix}\frac{D}{\theta} - \begin{bmatrix}0.797\\1.197\end{bmatrix}\left(\frac{D}{\theta}\right)^{1/3}\left[L^{2/3} - \left(\frac{D}{\theta}\right)^{2/3}\right]\right\}. \tag{23}$$

Both portions of the tilt variance are added to determine the overall tilt variance:

$$\sigma_T^2 = \sigma_\parallel^2 + \sigma_\perp^2 \approx \frac{6.08C_n^2}{D^{1/3}}\left[2L + 0.3077\frac{D}{\theta} - 1.9935\left(\frac{D}{\theta}\right)^{1/3}L^{2/3}\right] \qquad \theta > D/L. \tag{24}$$

As before, one could solve for $\theta$, this time numerically, to determine the tilt isoplanatic angle for $\theta > D/L$.

### *2.5. Scintillation anisoplanatism*

Stars twinkle, but the moon and even the planets do not twinkle in the night sky because their angular extents are much larger than the scintillation independence angle. In weak turbulence, the angle at which two point sources scintillate independently was postulated by Fried to be $\theta_{\chi_{ind}} = 0.8(Lk)^{-1/2}$, [19] corresponding to a separation distance of $d_{\chi_{ind}} = 0.8\,(L/k)^{1/2}$. This relation is very similar to the correlation width $\rho_c$ defined as the $1/e^2$ point of the normalized irradiance covariance function. [14] Since $\rho_c$, for weak turbulence varies between 1 to 3 Fresnel zones $(L/k)^{1/2}$ depending on beam size, we refer to it here in this work as simply [14]

$$\rho_c = \sqrt{L/k}. \tag{25}$$

For strong turbulence ($\mathscr{R}_{sph} \gtrsim 0.25$) the scintillation saturates and the correlation width of irradiance fluctuations $\rho_c$ is driven by the spatial coherence radius $\rho_0$ and the scattering disk $L/(k\rho_0)$.

The spherical wave Rytov number is

$$\mathscr{R}_{sph} = 0.5631k^{7/6}\int_0^L C_n^2(z)(L-z)^{5/6}\left(\frac{z}{L}\right)^{5/6}\mathrm{d}z \tag{26}$$

$$\approx \sigma_\chi^2 \qquad \mathscr{R}_{sph} \lesssim 0.25 \tag{27}$$

$$\gtrsim \sigma_\chi^2 \qquad \mathscr{R}_{sph} \gtrsim 0.25. \tag{28}$$

For weak turbulence the spherical wave Rytov number $\mathscr{R}_{sph}$ is equal to the log-amplitude variance calculation using this Rytov approximation. Since the scintillation saturates with strong turbulence, the Rytov number does not equal the log-amplitude variance.

#94855 - $15.00 USD Received 9 Apr 2008; revised 24 Jun 2008; accepted 27 Jun 2008; published 3 Jul 2008

The correlation width $\rho_c$ is often used to describe the receiver size at which aperture averaging occurs as the receiver size increases. Here, we use the principle of reciprocity to determine the angular separation of the transmitters and refer to this relation as the scintillation correlation angle as $\theta_{\chi_c} = (Lk)^{-1/2}$. The values of this angle $\theta_{\chi_c}$ for propagation lengths of 100 km and 29 km at $\lambda = 1.55$ $\mu$m are 1.57 $\mu$rad and 2.91 $\mu$rad, respectively.

### *2.6. Considerations of isoplanatic and anisoplanatic effects*

As mentioned in Section 2.2, the anisoplanatic condition can be determined by analyzing the structure functions of the effects. In previous work, Louthain determined analytic log-amplitude and phase structure functions for a horizontal path [22]

$$D_\chi(d) = 3.089\left(\frac{L_0}{r_0}\right)^{5/3}\int_0^\infty \left[1 - J_0\left(\frac{\kappa d}{L_0}\right)\right]\left[1 - \frac{2\pi L_0^2}{\lambda L\kappa^2}\sin\left(\frac{\lambda L\kappa^2}{2\pi L_0^2}\right)\right]\frac{\kappa \mathrm{d}\kappa}{(\kappa^2+4\pi^2)^{11/6}}, \quad (29)$$

and

$$D_\psi(d) = 3.089\left(\frac{L_0}{r_0}\right)^{5/3}\int_0^\infty \left[1 - J_0\left(\frac{\kappa d}{L_0}\right)\right]\left[1 + \frac{2\pi L_0^2}{\lambda L\kappa^2}\sin\left(\frac{\lambda L\kappa^2}{2\pi L_0^2}\right)\right]\frac{\kappa \mathrm{d}\kappa}{(\kappa^2+4\pi^2)^{11/6}}, \quad (30)$$

where $J_0$ is the zeroth order Bessel function of the first kind and the von Kármán PSD from Eq. (1) was used to model the turbulence. Here, we plot those equations and the corresponding isoplanatic and anisoplanatic distances in Fig. 1. Starting with the phase effects annotated in green, the isoplanatic angle occurs when the phase structure function is unity. As the separation widens, the tilt effects are isoplanatic until the tilt isoplanatic angle is reached. The only significant difference in these phases is due to the higher-order phase. Finally, at separations on the order of $2L_0$ all of the phase effects including tilt are anisoplanatic between the two paths. The amplitude effects are shown in blue. At about $2\rho_c$ the structure function reaches a maximum and settles into a value of two times the mean square log-amplitude variance, as the amplitude effects become uncorrelated. These separations are determined by the Fresnel zone $(L/k)^{1/2}$ and are consistent with results for weak turbulence, i.e. Rytov number $\mathscr{R}_{sph} < 0.25$ mentioned in Section 2.5. [14] For Anguita's stronger turbulence ground-to-ground propagation scenarios where $\mathscr{R}_{sph} = 1.6$ these uncorrelated separation distances were greater (approximately 6 $\rho_c$) due to the long correlation tail of the strong turbulence. [7, 14]

Now that we have the relations for isoplanatic and anisoplanatic effects, we compare these angles for different scenarios in Fig. 2. Horizontal propagation near the ground is shown in plot (b). If we separate transmitters in the ground-to-ground scenario by the phase-independence angle, then tracking might not be required. As long as there is a sufficient number of transmitters, the beams would wander independently with at least one beam on the receiver at any given moment. The fixed pointing angle could be determined by maximizing the long-term irradiance for each beam. The isoplanatic angle and the scintillation correlation angle cross at about 2.5 km. For propagations beyond the cross-over point scintillation is more correlated than phase effects. In plot (c), these terms cross, too, this time after propagating about 100 km. This also corresponds very well with Fig. 1 where the isoplanatic angle and the scintillation correlation angle nearly coincide with $\theta_0$ slightly smaller than $\theta_{\chi_c}$ for the 100 km air-to-air scenario.

For a mobile transmitter (Tx) and/or receiver (Rx), the beams must be tracked. For these tracked-beam cases in Fig. 2(c) air-to-air path, (d) air-to-ground path, and (e) ground-to-air path, separations beyond the isoplanatic angle up to approximately the tilt isoplanatic angle should average out the higher-order phase effects. Separations larger than the tilt isoplanatic

#94855 - $15.00 USD Received 9 Apr 2008; revised 24 Jun 2008; accepted 27 Jun 2008; published 3 Jul 2008

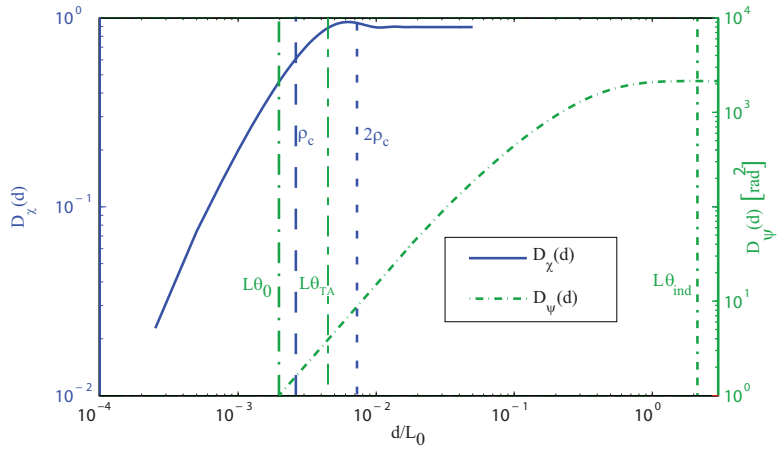


Fig. 1. The phase and amplitude structure functions are plotted for a 100 km horizontal propagation at 10 km altitude, with angularly separated beams. The strength of turbulence, $L_0/r_0 = 286$ and $L_0^2/(\lambda L) = 23225$.

angle will require separate trackers. This occurs for longer propagations and near-transmitter turbulence, since the phase tilt effects are large due to the long lever arm of the turbulence. Small isoplanatic and tilt-isoplanatic angles occur for propagations longer than 100 km in plot (c) and for the ground-to-air propagation shown in plot (e). In plot (d) describing the air-to-ground scenario, the correlation angles get smaller as the propagations get longer, but as the altitude of the transmitters gets above the turbulence at about 12 km, the angles remain relatively similar.

## 3. Simulation set-up and validation

Next, we determined how much multiple transmitters improve BER performance by conducting simulations for different scenarios and separation distances. The turbulence effects explored subsequently in simulated scenarios were represented by random optical field screens with the correct statistics placed along the path. The layers for this research were chosen to simulate the continuous model so that several low-order moments of the layered model match the continuous one. In this research, ten random phase screens were used to model the turbulence along varying-turbulence-strength paths and five screens along the constant-turbulence-strength paths. The layered analytic analytic planar and spherical coherence diameter $r_0$, planar and spherical Rytov numbers $\mathscr{R}$, and isoplanatatic angle $\theta_0$ matched within 1% of the full path continuous atmospheric turbulence parameters. Table 1 summarizes the atmospheric parameters for the simulations used to calculate the BER. In the simulations that follow a Gaussian beam with a $1/e$ field radius $w_0 = 2.5$ cm propagates to the receiver aperture with a Fresnel ratio of $\Lambda_0 = 2L/(kw_0^2)$. Andrews and Phillips call beams with $\Lambda_0 \gtrsim 100$ approximately spherical and $\Lambda_0 \lesssim 0.1$ approximately planar. Therefore, the equations in previous sections where a point source or spherical wave are used are a reasonable approximations, especially for the air-to-air propagation. Earlier, the von Kármán turbulence power spectrum was used to model the phase effects.

Andrews and Phillips' modified turbulence power spectrum is used in the simulations performed in this research because it includes $L_0$ and $l_0$, and gives the best agreement with collected atmospheric data for phase and *amplitude* effects. [14] The Hufnagel-Valley turbulence profile was used in this research with the parameters set to the HV-57 moderate turbulence strength (i.e. turbulence at the ground is $A = 1.7 \times 10^{-14}\text{m}^{-2/3}$ and the effective wind at alti-

#94855 - $15.00 USD Received 9 Apr 2008; revised 24 Jun 2008; accepted 27 Jun 2008; published 3 Jul 2008

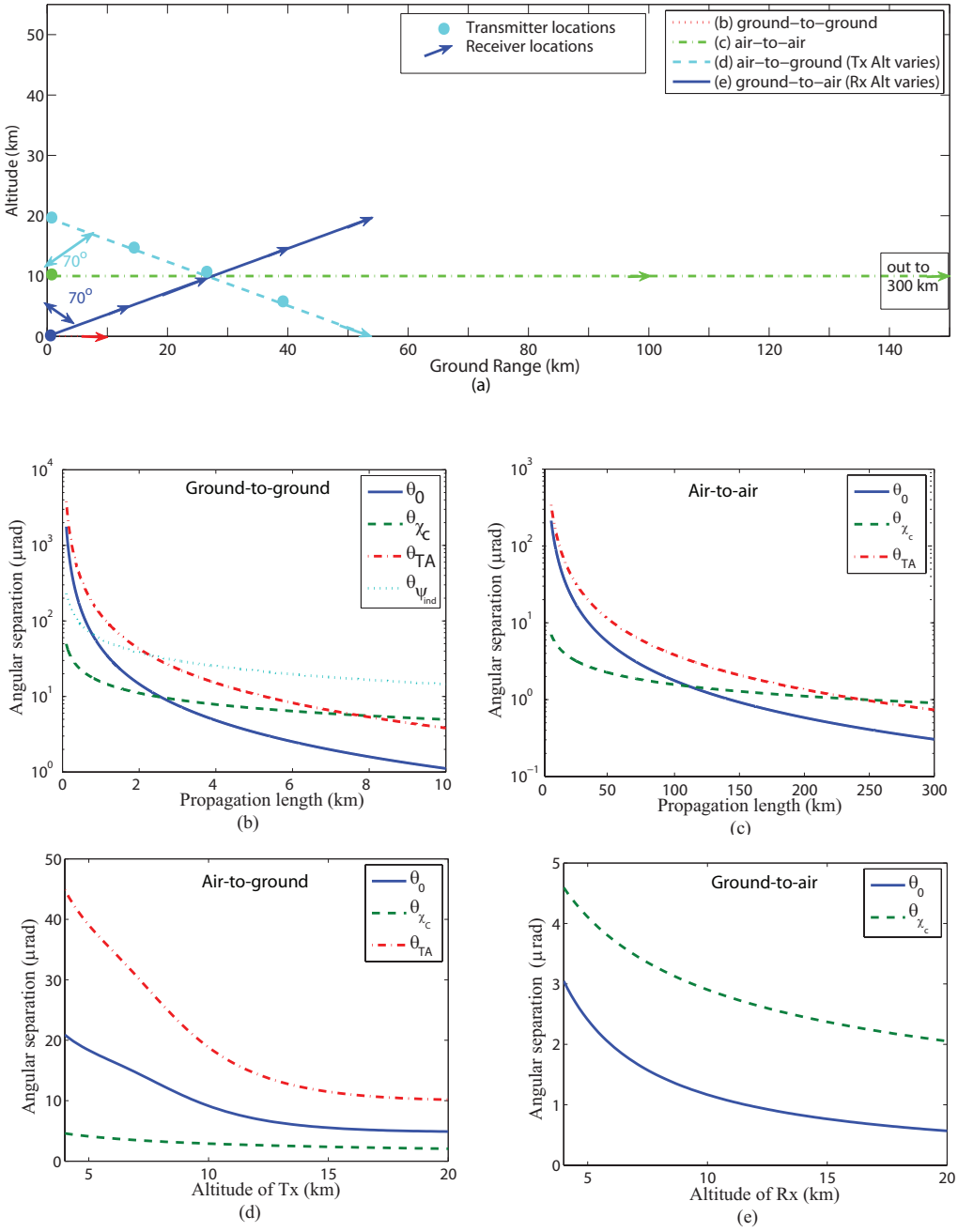


Fig. 2. (a) Scenarios for plots b-e are shown pictorially. Phase isoplanatic angle ($\theta_0$), scintillation correlation angle ($\theta_{\chi_c}$), tilt isoplanatic angle ($\theta_{TA}$), and phase uncorrelated angle ($\theta_{\psi_{ind}}$) are shown for a receiver diameter of $D_R = 20$ cm. (b) Horizontal propagation: altitude $h = 1$ m, $L_0 = 40$ cm, $C_n^2 = 10^{-14}$ m$^{-2/3}$, and $L = 0$ to 10 km. (c) Horizontal propagation: altitude $h = 10$ km, $L_0 = 100$ km, $C_n^2 = 10^{-17}$ m$^{-2/3}$, and $L = 0$ to 300 km. (d) Air-to-ground path: Transmitter height $H_{Tx} = 4$ to 20 km, zenith angle $\xi = 70°$, and receiver height $H_{Rx} = 0$ km for HV-57 profile. (e) Ground-to-air path: $H_{Tx} = 0$ km, zenith angle $\xi = 70°$, and $H_{Rx} = 4$ to 20 km for HV-57 profile.

#94855 - $15.00 USD Received 9 Apr 2008; revised 24 Jun 2008; accepted 27 Jun 2008; published 3 Jul 2008

Table 1. Atmospheric Parameters for the scenarios used in the BER calculations.

| Scenario | $r_{0_{pl}}$ (cm) | $r_{0_{sph}}$ (cm) | $\mathscr{R}_{pl}$ | $\mathscr{R}_{sph}$ | $\theta_0$ ($\mu$rad) | $\theta_{TA}$ ($\mu$rad) | $\Lambda_0$ |
|---|---|---|---|---|---|---|---|
| ground-to-ground | 2.5 | 4.5 | 1.08 | 0.437 | 3.5 | 11.7 | 3.2 |
| ground-to-air | 10 | 85 | 0.911 | 0.0461 | 1.2 | | 11 |
| air-to-air | 23 | 41 | 0.384 | 0.155 | 1.3 | 3.0 | 79 |

tude is $W = 21$ m/s).

We used modal based Fourier-series (FS) phase screen generation, since it allows for better low spatial frequency representation than other techniques. [12,20–23] This modal phase screen is defined for all space and need only be evaluated at the grid points of interest. This approach is particularly effective when calculating the fields of widely spaced beams over long periods of time. Although, in this work random realizations of turbulence are used in the simulations, since we assume the turbulence is an ergodic random process. Here, logarithmically-spaced frequencies are used, as recommended in an MZA report by Magee to take advantage of the modal-based representation. [18] The FS expansion of the phase can be approximated by [21]

$$\hat{\phi}(\mathbf{x}) = \sum_{n=-(N-1)}^{N-1} \sum_{n'=-(N-1)}^{N-1} c^{\phi}_{n,n'} \exp\left\{ j2\pi \left( \frac{nx}{D_p} + \frac{n'y}{D_p} \right) \right\}, \tag{31}$$

where the phase is represented in a square of dimension $D_p$ and $c^{\phi}_{n,n'}$ is the FS coefficient for the spatial frequency $\mathbf{f} = \hat{\mathbf{x}}n/D_p + \hat{\mathbf{y}}n'/D_p$. The terms $\hat{\mathbf{x}}$ and $\hat{\mathbf{y}}$ are the $x-$ and $y-$directed unit vectors, and $x$ and $y$ are the components of the spatial vector $\mathbf{x}$.

Split-step Fresnel propagations are performed for a $w_0 = 2.5$ cm collimated Gaussian beam. Great care was taken to adequately sample the Fresnel propagation between the screens as well as the turbulence effects as the beam propagates. We satisfied sampling constraints to avoid aliasing in the beam as well as the quadratic phase term in the Fresnel propagation. [24] The most restrictive constraint was satisfied by performing multiple partial propagations (i.e. split step propagations) to propagate the full distance.

We validated the simulations to ensure the calculations are representative of the diffraction and atmospheric turbulence effects. For each of the propagation lengths, the irradiance and phase of the Gaussian beams after propagating through a vacuum matched the analytical solution. The structure function of each of the phase screens was also consistent with the theoretical values. The scintillation index at the receiver for a simulated point source was consistent with the Rytov approximation for scintillation. For each of the turbulence simulations, the measured long-term spot size was consistent with the analytic spot size. These results confirmed the simulation operated as expected and should adequately model the turbulence.

## 4. Modeling receiver noise sources

Modeling receiver noise sources is essential to accurately representing a communication system. Two fundamental noise sources for optical receivers are the signal-level-dependent shot noise and the temperature-dependent Johnson noise. Shot noise is fundamentally a Poisson random process as the photo-electrons are generated for random arrivals of photons. The number of photons per bit is well over 100 in all of the cases studied here. Furthermore, as the captured power approaches zero, the shot noise approaches zero much faster than the signal. Therefore, shot noise current statistics are well approximated as a zero-mean Gaussian random process [26, 27]. The mean-square current due to shot noise is given by [28]

$$\mathrm{E}\left\{ i^2_{shot} \right\} = \sigma^2_{shot} = 2q\, i_S B = \frac{2\eta q^2 P B}{h\nu}, \tag{32}$$

#94855 - $15.00 USD Received 9 Apr 2008; revised 24 Jun 2008; accepted 27 Jun 2008; published 3 Jul 2008

where $q = 1.602 \times 10^{-19}$ C is the elementary charge, $i_s$ is the signal current, $B$ is the electrical bandwidth, $\eta$ is quantum efficiency (electrons/photon), $P$ is optical power at the detector (Watts), $h = 6.626 \times 10^{-34}$ J·s is Planck's constant, and $\nu$ is optical frequency (Hz). The product $h\nu$ gives the energy in joules of a single photon. The signal current is assumed to be constant during any given integration period corresponding to a single bit. Comparing the frequency of atmospheric change ($<$ kHz) with bandwidths studied ($>$ MHz), this is a reasonable assumption.

Johnson noise current is typically modeled as a zero-mean Gaussian random variable, with mean-square current determined by [28]

$$\mathrm{E}\left\{i_{elec}^2\right\} = \sigma_{elec}^2 = \frac{4KTB}{R} \quad , \tag{33}$$

where $K = 1.381 \times 10^{-23}$ J/K is Boltzmann's constant, $T$ is temperature of the electronics (K), and $R$ is the effective input resistance (ohms). These are the primary noise sources in the receiver.

There is also noise due to the type of amplifier or gain mechanism. In this research the received optical signal is coupled into an erbium-doped-fiber amplifier (EDFA). The advantage of the EDFA is the capability to achieve high gain at very high bandwidths. In addition, the gain in an EDFA saturates, affording some gain control to reduce optical signal variation. EDFA noise can be modeled as a signal-dependent amplified stimulated emission (ASE) noise source given by [26]

$$\begin{aligned} \mathrm{E}\left\{i_{ASE}^2\right\} &= 4q^2 n_{sp}\eta_{in}\eta_{out}^2 G(G-1)\frac{P}{h\nu}B \\ \sigma_{ASE}^2 &= 4n_{sp}\eta_{out}q(G-1)i_s B, \end{aligned} \tag{34}$$

where $G$ is the gain, $\eta_{in}$ and $\eta_{out}$ are the input and output losses, and $n_{sp}$ is the spontaneous emission factor. Other gain mechanisms like avalanche photo diodes (APD) are limited to about 100-200 GHz gain-bandwidth product, whereas an EDFA with a PIN photodiode would be at least an order of magnitude higher. [26] For lower bandwidths an APD is advantageous due to a much higher coupling efficiency.

## 5. Simulation approach

The receiver consists of a 20-cm-diameter lens with a 1 m focal length focused onto a single-mode optical fiber. The fiber core's diameter was 3 $\mu$m and the numerical aperture (NA) was 0.20, consistent with a commonly available EDFA. For the 100 km propagation the collimated Gaussian beam at the Rx is much larger than the aperture and since $r_0 > D$ the spot size at the focal plane of the lens is determined by $2.44\lambda f/D$, limited only by diffraction. For the ground-to-ground and ground-to-air cases the turbulence-induced spot size is approximately $2.44 f\lambda/r_0$, since $r_0 < D$ for those cases. See Table 1 and Fig. 3.

For the angularly-separated-beam scenario, two Gaussian beams are displaced half the separation distance in opposite y-directions and a linear phase is applied to "aim" both beams at the center of the receiver aperture. For the parallel-beam case, the two Gaussian beams are displaced, and each beam remains off-axis by half the separation distance.

A coarse tracking system was simulated for the transmitter and receiver for the ground-to-air and the air-to-air paths by implementing an ideal centroid tracker and adding random tracking system errors. The errors in the Tx tracker are driven by tilt isoplanatism $\sigma_{TA}^2$ due to the point-ahead angle, temporal errors $\sigma_{TT}^2$ in the controller, platform jitter $\sigma_{PJ}^2$, and measurement error $\sigma_{TM}^2$. Therefore the total transmitter tracker error is

$$\sigma_j^2 = \sigma_{TA}^2 + \sigma_{TT}^2 + \sigma_{PJ}^2 + \sigma_{TM}^2 \tag{35}$$

#94855 - $15.00 USD Received 9 Apr 2008; revised 24 Jun 2008; accepted 27 Jun 2008; published 3 Jul 2008

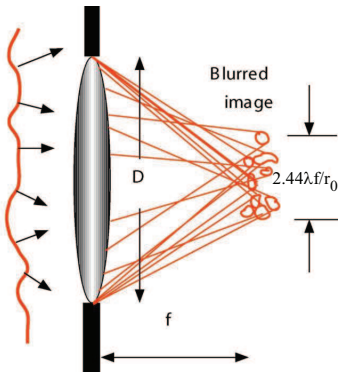


Fig. 3. In turbulence when $D > r_0$, the spot size is determined by $2.44\lambda f/r_0$. Where as when $r_0 > D$, the spot size is limited primarily by diffraction, leading to the tighter spot size of $2.44\lambda f/D$.

measured in rad$^2$. The tilt anisoplanatic error is driven by how close the separation angle is to the tilt isoplanatic angle. The temporal error is dependent on the bandwidth of the tracking system and the tilt measurement error depends upon the signal to noise ratio (SNR) of the tilt measurement. The platform jitter is driven by the residual vibrations of the transmitter and receiver. The receiver tracker error includes the last three terms of Eq. (35).

## 6. Simulation results

We ran simulations using independent random realizations of the appropriate turbulence statistics to determine the optimal separations for a two transmitter system for three scenarios: a ground-to-ground fixed transmitter and receiver 4 km link with a Rx and Tx height of 1 m, a ground-to-air ($h = 1$ m to 10 km) 30.2 km path with a zenith angle $\xi = 70^\circ$, and an air-to-air 100 km path at 10 km in altitude.

A number of performance measurements were calculated, but the differential irradiance variance between the two beams $\sigma^2_{\Delta irr} = \mathrm{E}\left\{(I_1 - I_2)^2\right\} - \mathrm{E}\left\{I_1 - I_2\right\}^2$ best indicated when adequate averaging would occur. [2, 3, 7] The larger the differential irradiance variance, the less correlated the irradiance fluctuations become. For uncorrelated beams this variance should approach two times the irradiance variance of a single beam. If the angular separation is much beyond this point, the power received at the detector or fiber is reduced due to the difference in the angle-of-arrival (AOA) of the beams. As parallel beams move farther off-axis, power reduces and the variability of the constituent beams increases. This effect increases the BER of the two-transmitter system driving the performance below the one-transmitter case. As shown in Fig. 4, beams approached uncorrelated irradiance variance at about 2-3 $\rho_c$ for angularly separated beams for both the air-to-air tracked system and the ground-to-air tracked system. In addition, for the air-to-air scenario this the amplitude structure function has a peak before settling into the asymptotic value of two times the irradiance variance of the single beam.

Then, we determined the BER for different scenarios, tracking systems, and separation distances. Plots are shown in Figs. 5-8. In calculating the BER, we used the probability mass function of the detected signal current (determined by the histogram of the received signal) and accounted for the shot, thermal, and ASE noise. Since the shot and ASE noise are signal-dependent, their variance changed for each independent realization, while the thermal noise variance was fixed. We solved for the optimal fixed threshold and determined the probabilities of missed detections and false alarms. The total power in the single-transmitter system was 1

#94855 - $15.00 USD Received 9 Apr 2008; revised 24 Jun 2008; accepted 27 Jun 2008; published 3 Jul 2008

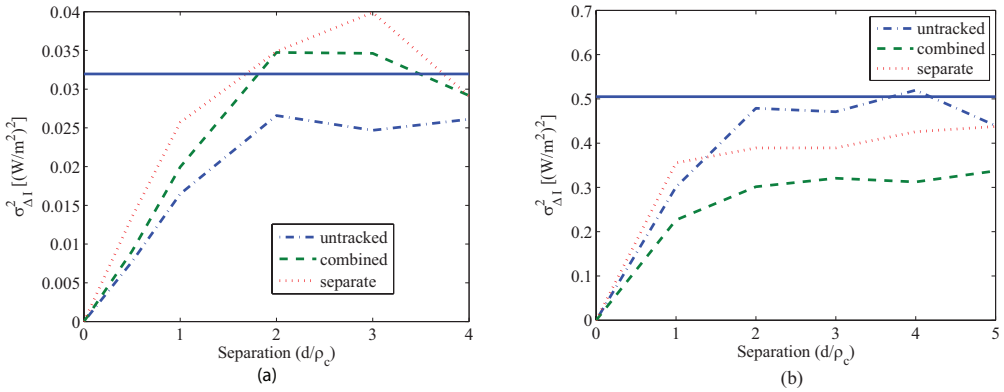


Fig. 4. Differential irradiance variance for two angularly separated beams. Irradiance is taken from the center of the untracked beams, separately tracked beams, and a single combined beam tracker. The solid blue line is two times the variance of on-axis irradiance of a single beam. The differential variance approaches two times this value as the separation increases. (a) Air-to-air path angular separation (b) Ground-to-air path angular separation.

Watt, and the total power in the double-transmitter system was also 1 Watt (0.5 Watts in each transmitter). For the BER charts, the gain of the EDFA remained constant at 30 dB. The signal level differences shown in the plots vary due to differences in propagation attenuation, coupling efficiencies, transmitter levels, etc., but do not depend on the gain of the EDFA.

First, we calculated the BER for the ground-to-ground path for single and double-transmitter systems. No tracking system was used in this case, and the beams walked off of the receiver often. To quantify this, note that the standard deviation of the beam walk-off was 9.5 cm and the short-term beam half-width was 8.3 cm. The differential tilt variance approached two times the single tilt variance in the direction parallel to the separation for very small separations (i.e. 3 cm), but for the perpendicular direction the required separation distance for uncorrelated phase was about 10 $\rho_c$ or about $d_{\psi_{ind}}/2$. This phenomenon is consistent with the differential tilt relations presented by Sasiela. [9] Figure 5 shows there was slight improvement for the double transmitter case over the single beam when the transmitters propagated in parallel, but no improvement for angular separations. Due to the inherent AOA for angularly separated beams, the peaks of the focal spots of both beams on average miss the fiber, reducing the coupling efficiencies. If the fiber core is small, as in this case, this could severely limit the coupling of both beams. Whereas with the parallel beams, the focal spots were on average on the center of the fiber, allowing for much better coupling.

Next, we calculated the BER of a tracked ground-to-air scenario. The BER charts in Fig. 6 show that there is an improvement afforded by using two transmitters of about 3 dB for the ideal tracker. Interestingly, two transmitters also improved performance for the non-ideal case for a tracker error of $\sigma_j = \lambda/(4D)$. Parallel beams were used with a center tracker system. For this case, Fig. 7 shows an improvement again for a tracking system with $\sigma_j = \lambda/(4D)$. This improvement reduces in both cases as the tracking system performance degrades.

Finally, the BER charts in Fig. 8 for the air-to-air 100 km path shows the best improvement for a separation distance of 2 to 3 $\rho_c$. This is consistent with the differential scintillation measurements. The largest improvement (approximately 4 dB) occurs for the finest tracking system. As the tracking degrades, the improvement due to the signal diversity decreases.

#94855 - $15.00 USD Received 9 Apr 2008; revised 24 Jun 2008; accepted 27 Jun 2008; published 3 Jul 2008

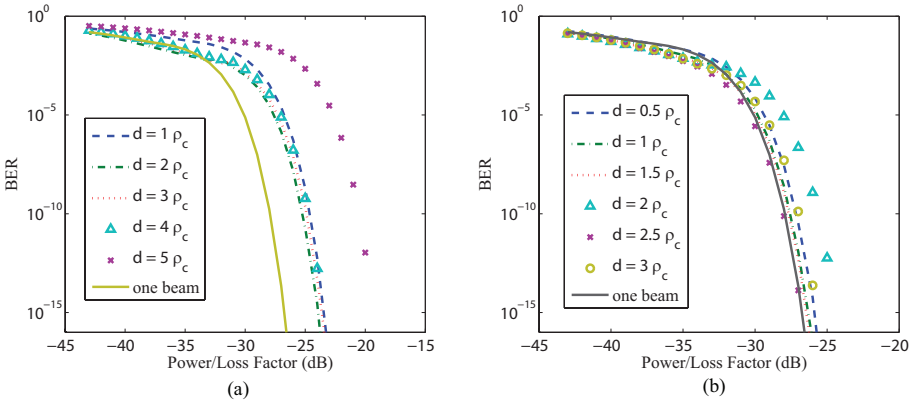


Fig. 5. These plots show the BER for a ground-to-ground link. In plot (a) the beams were angularly separated and in plot (b) the beams were separated, but traveled in parallel.

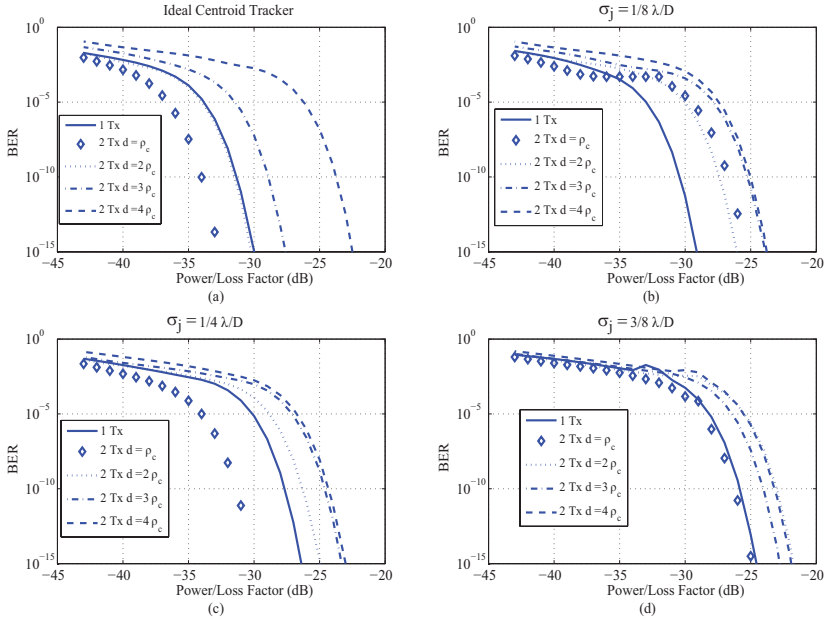


Fig. 6. Bit error rate for a ground-to-air link with angularly separated beams with various tracking systems (a) ideal centroid tracker, (b) $\sigma_j = \lambda/(8D)$, (c) $\sigma_j = \lambda/(4D)$, and (d) $\sigma_j = 3\lambda/(8D)$.

#94855 - $15.00 USD Received 9 Apr 2008; revised 24 Jun 2008; accepted 27 Jun 2008; published 3 Jul 2008

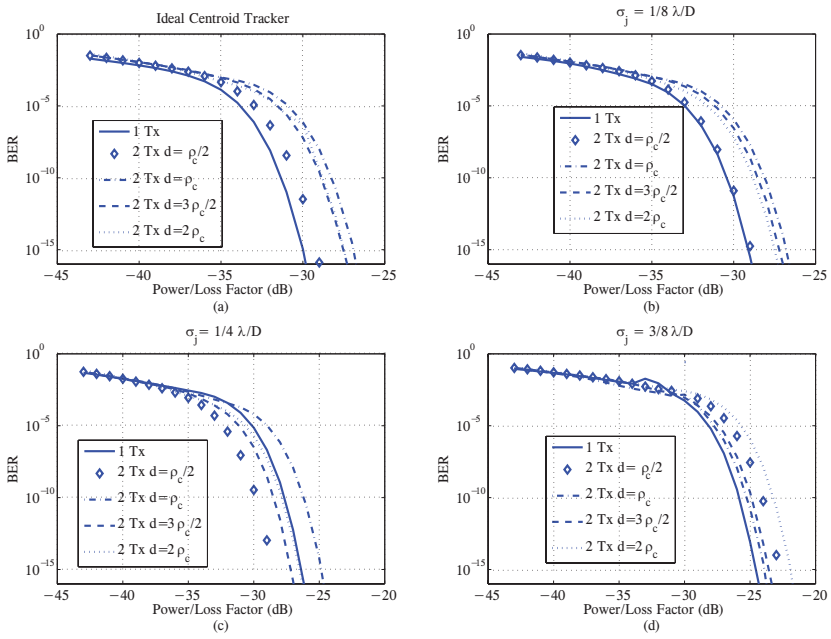


Fig. 7. Bit error rate for a ground-to-air link for parallel separated beams. Center beam tracker. Various tracking systems (a) ideal centroid tracker, (b) $\sigma_j = \lambda/(8D)$, (c) $\sigma_j = \lambda/(4D)$, and (d) $\sigma_j = 3\lambda/(8D)$.

## 7. Conclusions

Knowledge of the isoplanatic and uncorrelated angles of particular scenarios can enable multiple-transmitter systems to be configured to optimize the averaging effects. For a group of beams with one tracker, the optimal angular separation must be less than the tilt isoplanatic angle. In this regime, the scintillation and the higher-order phase effects can be averaged, and the beams wander together so that the tracking system can adequately track all of the beams at once. Beams separated beyond the tilt isoplanatic angle wander independently causing track errors and reduced signal levels.

For a multiple-transmitter untracked system, the outer scale and the mean-square phase play a large role in determining an appropriate separation angle. The likely application for an untracked system is a ground-to-ground last-mile communication system, since the system is stationary and the outer scale is small, allowing for reasonable separation distances.

The optimal separation in terms of reducing BER corresponded to 2-3 times $\rho_c$ for most of the scenarios. In most cases, the BER improvement for a two-transmitter system reduced as the tracking system degraded. For small focal-plane collectors like a single mode fiber, AOA plays a huge part in the received signal level. Not only is AOA variance an issue, the mean AOA can be a concern if beams are angularly separated. Since scintillation effects begin to decorrelate for fairly small separations, the transmitters only need to be separated by approximately $2\rho_c$ for most scenarios.

To illustrate the optimal separation only two beams were used, so the full impact of our approach has yet to be explored. Others have shown that four beams, for instance, can be very effective in a ground-to-ground link scenario. [7] This approach shows great potential in per-

#94855 - $15.00 USD Received 9 Apr 2008; revised 24 Jun 2008; accepted 27 Jun 2008; published 3 Jul 2008

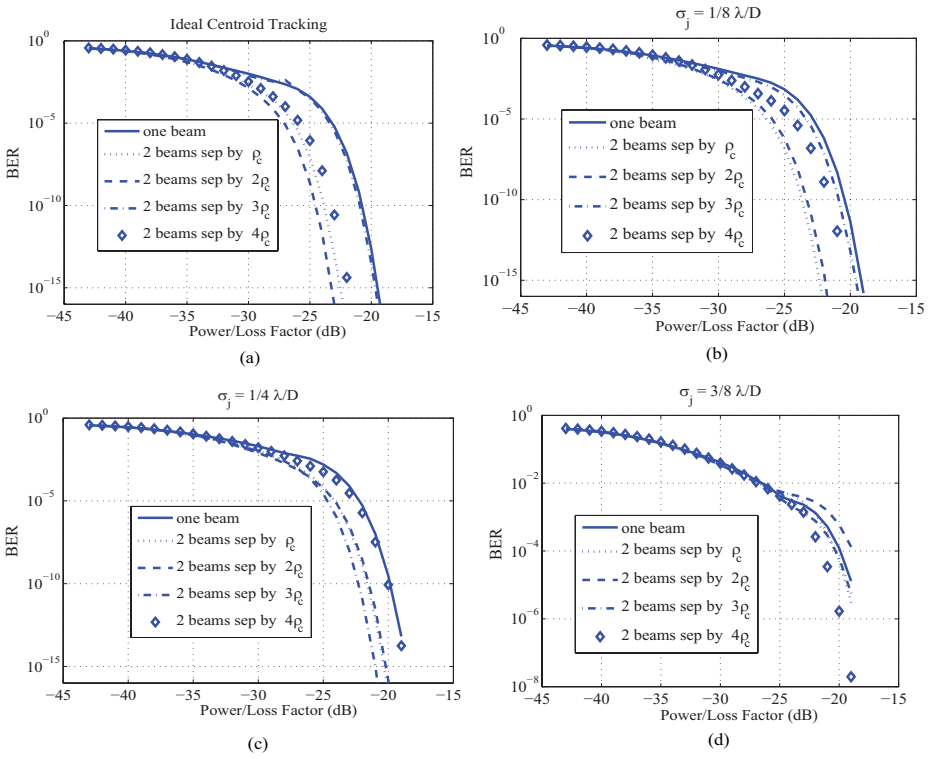


Fig. 8. Air-to-air 100km path at 10km altitude. Various tracking systems (a) ideal centroid tracker, (b) $\sigma_j = \lambda/(8D)$, (c) $\sigma_j = \lambda/(4D)$, and (d) $\sigma_j = 3\lambda/(8D)$.

formance and simplicity of implementation, especially when combined with signal-processing techniques. Accordingly, the next step in this research will be to determine the *temporal* benefits afforded by multiple anisoplanatic transmitters. We will investigate signal-fade properties of using multiple beams and potential trickle-down effects of coupling multiple beams with interleaving, forward error correction, and adaptive thresholding.


## Acknowledgment

Many of the theoretical relations presented here were developed by the late Dr. Richard J. Sasiela. He will truly be missed. The views presented in this paper are those of the authors and do not necessarily represent the views of the Department of Defense or its components.


#94855 - $15.00 USD Received 9 Apr 2008; revised 24 Jun 2008; accepted 27 Jun 2008; published 3 Jul 2008